JOURNAL OF NEUROTRAUMA 35:2104–2116 (September 1, 2018)

DOI: 10.1089/neu.2017.5394

Long-Term Functional and Structural Consequences of Primary Blast Overpressure to the Eye

Rachael S. Allen,[1,2,*] Cara T. Motz,[1,*] Andrew Feola,[1,2,] Kyle C. Chesler,[2] Raza Haider,[1] Sriganesh Ramachandra Rao,[3] Lara A. Skelton,[4] Steven J. Fliesler,[3,4] and Machelle T. Pardue[1,2]

Abstract

Acoustic blast overpressure (ABO) injury in military personnel and civilians is often accompanied by delayed visual deficits. However, most animal model studies dealing with blast-induced visual defects have focused on short-term (≤1 month) changes. Here, we evaluated long-term (≤8 months) retinal structure and function deficits in rats with ABO injury. Adult male Long-Evans rats were subjected to ABO from a single blast (approximately 190 dB SPL, ~63 kPa, @80 psi), generated by a shock tube device. Retinal function (electroretinography; ERG), visual function (optomotor response), retinal thickness (spectral domain–optical coherence tomography; SD-OCT), and spatial cognition/exploratory motor behavior (Y-maze) were measured at 2, 4, 6, and 8 months post-blast. Immunohistochemical analysis of glial fibrillary acidic protein (GFAP) in retinal sections was performed at 8 months post-blast. Electroretinogram a- and b-waves, oscillatory potentials, and flicker responses showed greater amplitudes with delayed implicit times in both eyes of blast-exposed animals, relative to controls. Contrast sensitivity (CS) was reduced in both eyes of blast-exposed animals, whereas spatial frequency (SF) was decreased only in ipsilateral eyes, relative to controls. Total retinal thickness was greater in both eyes of blast-exposed animals, relative to controls, due to increased thickness of several retinal layers. Age, but not blast exposure, altered Y-maze outcomes. GFAP was greatly increased in blast-exposed retinas. ABO exposure resulted in visual and retinal changes that persisted up to 8 months post-blast, mimicking some of the visual deficits observed in human blast-exposed patients, thereby making this a useful model to study mechanisms of injury and potential treatments.

Keywords: blast; electroretinogram; optomotor response; retina; visual function

Introduction

Blast-induced injuries with resultant brain trauma represent the signature injury of the campaigns in Iraq and Afghanistan (Operation Iraqi Freedom and Operation Enduring Freedom), with hundreds of thousands of soldiers being affected.[1,2] These injuries often include trauma to the eye and visual system. The mechanisms that cause tissue damage and dysfunction following blast exposure are not fully understood. There is no definititive way to diagnose, prevent, or treat blast injury. Compounding the issue of diagnosis is that many behavioral symptoms of blast injury, such as changes in mood, sleep disturbances, and cognitive difficulties, are also symptoms of post-traumatic stress disorder (PTSD), and the two can be co-morbid.[3] To better diagnose patients with blast injury, suitable metrics and biomarkers—which may include changes in the retina and visual function—are desperately needed.

During a blast event, sonic shockwaves (acoustic blast overpressure, ABO) radiate from the origin of the explosion and can cause injury to the brain, eyes, and multiple tissues and organ systems (i.e., polytrauma). Visual function can be compromised due to damage at any point along the visual pathway, from the cornea to the visual cortex.[4–7] In closed-globe injuries, where the eye remains structurally intact and without obvious penetrating injury, the damage may not be readily apparent and visual deficits may be occult and go unrecognized, particularly if the patient initially presents with normal visual acuity.[4,6] However, with time, the damage becomes manifest and persistent. Such progressive and chronic visual defects, including photosensitivity, accommodation issues, reading difficulties, decreased contrast sensitivity (CS), and visual field deficits,[6,8–10] occur in 52–68% of patients who have experienced one blast exposure[10,11] and 87.5% of patients with more than one blast exposure.[10] Additionally, patients with blast injuries may not present with a visual complaint until weeks, months, or even years after the injury.[5,6] The reasons for this remain unknown. However, the majority of animal model studies on blast injury to the eye typically are terminated by 4 weeks or earlier

[1]Center for Visual and Neurocognitive Rehabilitation, Atlanta VA Medical Center, Atlanta, Georgia.
[2]Biomedical Engineering, Georgia Institute of Technology, Atlanta, Georgia.
[3]Ophthalmology, Biochemistry, and Neuroscience Program, SUNY-University at Buffalo, Buffalo, New York.
[4]Research Service, VA Western NY Healthcare System, Buffalo, New York.
*The first two authors contributed equally.

post-blast, at which time visual function changes are only just beginning to appear.[12–16] Thus, there is an urgent need to increase our understanding of the mechanisms underlying the initiation and progression of the pathological sequelae post-blast to develop better methods for detection and optimal treatment strategies.

To determine the longitudinal progression of visual dysfunction after blast exposure, we used a relatively novel rat model of closed-globe ABO injury to the eye, employing a modified shock tube device originally developed by Newman and colleagues[17] to study blast injury to the auditory system. We characterized the changes in visual function and retinal structure in both the ipsilateral (proximal to the shock wave) and contralateral eyes, as well as changes in cognitive function and exploratory behavior following ABO exposure, in comparison with rats that had not been exposed to ABO. We hypothesized that blast overpressure exposure would result in structural and functional changes to the retina and visual system that would worsen with time.

Methods

Animals and experimental design

Adult male Long-Evans (Blue Spruce, HsdBlu:LE; Envigo) outbred rats were used in this study. At the time of blast, rats were approximately 3.5 months of age (420–450 g). Non-blast-exposed, age-matched male Long-Evans rats served as controls. Animals were housed under normal 12:12 light:dark conditions (ambient lighting, approximately 40 lux), with chow and water provided *ad libitum*, and ambient room temperature (approximately 22–25°C). All animal procedures were approved by the respective Institutional Animal Care and Use Committees (IACUCs) of both the VA Western New York Healthcare System (VAWNYHS) and the Atlanta VA Medical Center, and conformed to the Association for Research in Vision and Ophthalmology's (ARVO's) *Statement for the Use of Animals in Ophthalmic and Visual Research* and *Guide for the Care and Use of Laboratory Animals* (National Research Council of the National Academies, United States, 8th edition).

Blast injury was performed at the Buffalo VA Medical Center. After one month of recovery, animals were shipped to the Atlanta VA Medical Center for functional assessments, including electroretinography (ERG), optomotor response (OMR), spectral domain–optical coherence tomography (SD-OCT), and Y-maze testing. Unless otherwise specified, all functional outcomes measures were performed at 2, 4, 6, and 8 months post-blast exposure. One rat was excluded from the 8-month Y-maze test because it was too large to move in the maze. Also, some OCT scans were deemed unusable due to blurring of the images caused by breathing movements; therefore, those data were excluded from the analysis. At the termination of experimental procedures, animals were euthanized either by decapitation or perfusion, depending on the specific application; these procedures were conducted in accordance with the recommendations of the Panel on Euthanasia of the American Veterinary Medical Association (AVMA).

Acoustic blast overpressure (ABO) exposure

ABO exposure was performed under closed-globe conditions, using a modified shock tube device (Fig. 1A,B) described in detail elsewhere.[17] Briefly, prior to blast exposure, rats were anesthetized (intramuscular [IM] injection) with a mixture of ketamine (75 mg/kg) and xylazine (15 mg/kg), and topical anesthetic (proparacaine hydrocholoride, 0.5% ophthalmic solution, Akorn, Inc.; 1–2 drops/eye) was instilled into each eye. Rats were then exposed to a single acoustic blast, with a sound pressure level of approximately 190 dB SPL (sound pressure ~63 kilopascals [kPa]), using an 80-psi backpressure load of compressed nitrogen in the shock tube. Pressure (80 psi) was measured with a standard pressure gauge (similar to that used on compressed gas cylinder regulators) mounted on the shock tube body. Sound pressure (db SPL) was measured using a pressure sensor (Model 137A23 ICP Pressure Sensor; PCB Piezotroncis) placed at the outlet of the shock tube. A brass foil diaphragm inserted near the mid-section of the shock tube and held in place by O-rings (Fig. 1B) provided resistance to allow buildup of nitrogen gas behind it, which was electronically controlled by a computer (Fig. 1C). When the criterion pressure inside the shock tube was achieved, a computer-controlled, solenoid-driven arrow inside the tube was thrust forward, rupturing the foil (see Fig. 1G) and instantaneously releasing the backpressure, with resulting generation of an acoustic shockwave from the shock tube outlet. During blast exposure, rats were housed in a specially designed animal holding chamber (fabricated from high-density plastic on a 3D printer) bolted to the supporting table such that only the head was exposed (Fig. 1D). The outlet end of the shock tube muzzle was positioned approximately 2.5 in from the head (Fig. 1E,F), and the blast was directed at the right eye (OD) only, perpendicular to the body axis. The head was not physically constrained; however, as shown in Figure 1F, a large pillow was placed against the contralateral (left) side of the head, to reduce the extent of impact and recoil.

Following blast exposure, topical antibiotic ointment (gentamycin sulfate, 0.3% ophthalmic ointment; Akorn, Inc.) was administered to each eye to maintain corneal hydration, and animals were returned to their cages in a recovery area; body temperature was maintained by placing the cages on heating pads, and animals were closely monitored for viability and signs of distress at regular intervals thereafter. In initial experiments, animals were allowed to recover naturally over the course of several hours. However, the protocol was subsequently altered (with veterinarian guidance and IACUC approval), such that anesthesia was reversed by injection of Antisedan® (1 mg/kg, intraperitoneally [IP]; Pfizer Animal Health) within 10 min following blast exposure. Blast-exposed animals were given buprenorphine (0.05 mg/kg, subcutaneous [SC] injection) as an analgesic approximately 30–40 min after Antisedan® administration and again 24 h post-blast. (Note: Empirically, we have found it extremely important not to administer buprenorphine sooner than 30 min post-Antisedan® treatment, due to respiratory suppression by buprenorphine, which can be lethal.)

Rats were allowed to recover for at least 24 h prior to any further use. In the course of these studies, we encountered unanticipated death of some animals: five rats died shortly after blast exposure or were humanely euthanized following ruptured-globe injury to the contralateral eye (concussive impact with the wall of the animal housing chamber); one blast-exposed rat died over a month after injury of unknown causes but before the start of any assessments; and two blast-exposed and seven control rats died in the course of functional testing due to failure to recover from anesthesia.

Electroretinography (ERG)

ERG was performed to measure retinal function, as previously described.[18] In brief, rats were dark-adapted overnight and then anesthetized with a ketamine (60mg/kg)/xylazine (7.5 mg/kg) mixture (for rats ≥6-months old, rats requiring additional anesthesia were given a ketamine-only booster). Corneas of the animals were anesthetized topically with tetracaine (1%) and pupils dilated with tropicamide (1%). Reference and ground-needle electrodes were placed subcutaneously in each cheek and in the tail, respectively. Retinal responses were measured directly using custom gold-loop electrodes that were placed on the corneal surface of each eye under a layer of methylcellulose. ERG stimuli consisted of five steps of full-field flashes presented under scotopic conditions in a Ganzfeld dome (–3.0 to 2.1 log cd sec/m^2) using a commercial system (UTAS Big Shot, LKC Technologies, Gaithersburg, MD). Responses were bandpass filtered (0.3–500 Hz) with a 250 msec recording length. Retinal function was allowed to recover between each step with interflash intervals increasing from 2 to 70 sec as light intensity increased. Following the fifth step, rats were light

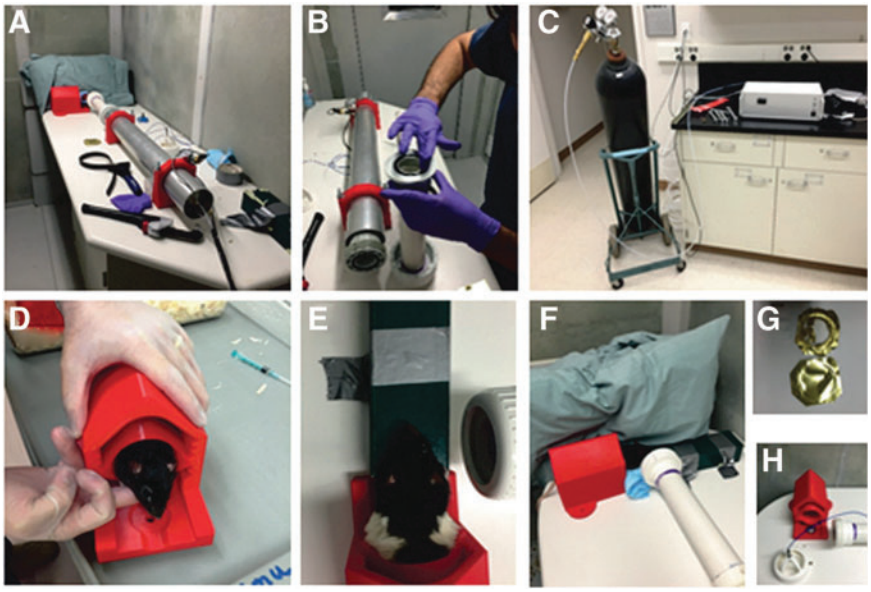

FIG. 1. Acoustic blast overpressure setup. **(A,B)** Shock tube assembly. **(C)** Compressed gas tank and controller unit, outside blast chamber. **(D-F)** Placement of rat in holder and positioning prior to blast. **(G)** Brass foil diaphragm before (lower image) and after (upper image) blast. **(H)** Pressure sensor assembly, end of shock tube, and animal holder.

adapted for 10 min (30 cd/m^2) and then presented with a flickering light stimulus (2.0 log cd sec/m^2 at 6 Hz). Amplitudes and implicit times were measured for a-waves (baseline to trough), b-waves (trough to peak), flicker b-waves (trough to peak), and oscillatory potentials (OP). OPs were filtered off-line using a 75–500 Hz filter (EM for Win version 8.1.2, LKC Tecnologies). Reported OP amplitudes and implicit times are the averages of OP2 from the brightest flash stimuli. Reported amplitude averages across time are for the brightest flash stimuli.

Optomotor response (OMR)

Visual function of rats was tested using a virtual optokinetic tracking system (OptoMotry®; Cerebral-Mechanics, Lethbridge, AB, Canada) as previously described.[19,20] In brief, the rat is placed on a platform in the middle of a virtual-reality chamber consisting of four computer flatscreen monitors that display vertical sine wave gratings rotating at a speed of 12 deg/sec. The rat is monitored in real time with a video camera, and the experimenter monitors the presence or absence of reflexive head movements (tracking) in response to rotating gratings moving in a clockwise or counterclockwise direction. Spatial frequency (SF) and CS thresholds are calculated automatically by the OptoMotry software using a staircase paradigm. For SF assessment, gratings began with a SF of 0.042 cyc/deg with 100% contrast, and the SF was adjusted while contrast remained constant. For CS assessment, measurements began at 100% contrast and were then decreased accordingly, while SF was kept constant at 0.064 cy/deg, the peak of the CS curve for the rats at baseline. The reported CS was calculated as a reciprocal of the Michelson contrast from the screen's luminance (i.e., [maximum + minimum] / [maximum – minimum]), as previously described.[21]

Spectral domain-optical coherence tomography (SD-OCT)

A SD-OCT system (Bioptigen 4300, Lieca Microsystems, Buffalo Grove, IL) was used to evaluate the structural integrity of the retina. Following anesthesia (as per above), corneal anesthesia (tetracaine1%), and pupil dilation (tropicamide 1%), the rat eye was positioned in front of the SD-OCT system. A 3-mm radial scan centered at the optic nerve was then taken for each eye and 1000 a-scans per b-scan were imaged. A total of four b-scans consisting of 24 individual frames per scan were collected; only the superior to inferior and nasal to temporal scans were analyzed.

B-scan images of all eyes were assessed manually by a trained technician using a customized MATLAB program (Mathworks, Matlab R2017a, Natick, MA). Markers were placed at the boundaries of each layer, and the program computed the thickness (in microns) of each retinal layer: retinal nerve fiber layer (RNFL), inner plexiform layer (IPL), inner nuclear layer (INL), outer plexiform layer (OPL), outer nuclear layer (ONL), external limiting membrane (ELM), inner segments/outer segments (IS/OS), and retinal pigment epithelium (RPE). Total retinal thickness (TRT) was computed by finding the difference between the inner point of the RNFL and the outer point of the RPE. B-scan images were taken at four different orientations within the eye: superior, inferior, nasal, and temporal. Additionally, for each quadrant, thickness measurements were taken at two different distances from the optic nerve head (ONH): 0.5 mm and 1.2 mm. Because no statistical differences were found between quadrant or distance away from the ONH, quadrants were averaged and only the 0.5-mm measurements were analyzed.

Cognitive function testing (Y-maze)

Based on methods previously described by Maurice and colleagues,[22] the Y-maze was used to evaluate cognitive function. Each rat was placed in one arm of a Y-maze apparatus (San Diego Instruments, San Diego, CA) and allowed to freely explore for a total of 8 min. During that time, the sequence and entries into each arm were recorded. An alternation was measured as consecutive entries into three different arms (i.e., ABC) on overlapping triads in which all arms were present. The final spatial alternation score was a percentage calculated by taking the actual number of successful alternations divided by the number of total possible alternations that could have been achieved (total number of entries minus two). Percentage of correct alternations and total number of entries were analyzed.

Immunohistochemisty

At the end-point of the experiment (8 months post-blast exposure), rats were euthanatized (decapitation), and eyes ($n = 6$–8 per

condition) were enucleated and ''fixed'' by immersion in phosphate-buffered saline (PBS) 3.7% (w/v) formaldehyde (prepared from paraformaldehyde; Electron Microsopy Sciences [EMS]) overnight at 4°C, and then rinsed with chilled PBS 3 times. Fixed eyes were cryoprotected overnight at 4°C by immersion in 30% (w/v) sucrose in PBS, and then embedded in TissueTek® Optimal Cutting Temperature (OCT) Compound (EMS). Cryosections (10-μm thickness) were collected onto glass Gold Seal™ UltraFrost™ microscope slides (ThermoFisher Scientific), using a Leica® Model CM3050S Cryostat (Leica Microsystems), taking sections in a direction parallel to the vertical meridian and cutting through or proximal to the ONH. Tissue cryosections were then subjected to brief immersion in PBS containing 100 mM glycine (to block free aldehyde groups), followed by two brief rinses in PBS. To block non-specific binding of secondary antibodies, sections were treated with non-immune (normal) goat serum (5% [v/v] in PBS, supplemented with 0.025% [v/v] saponin [Sigma-Aldrich], 0.1% [w/v] bovine serum albumin [BSA; Sigma-Aldrich], and 0.5% [w/v] fish skin gelatin [Sigma-Aldrich]). Cryosections were then briefly rinsed with PBS containing 0.1% Triton-X 100 (Sigma-Aldrich), and exposed (overnight at 4°C in a humidified chamber) to a rabbit polyclonal antibody raised against glial fibrillary acidic protein (GFAP; Dako #Z0334; 1:1000, diluted in PBS supplemented with 0.1% [w/v] BSA). Negative controls employed either no primary antibody, or non-immune immunoglobulin G (IgG; 10 μg/mL) from goat serum; neither showed any positive immunolabeling (data not shown). After one rinse with PBS, tissue sections were incubated for 1 h at room temperature with fluor-conjugated secondary antibody ($F(ab')_2$-goat anti-rabbit IgG [H+L], conjugated with AlexaFluor® 647 [Invitrogen, #A21246; 1:250, diluted as for primary antibody]). Slides were rinsed with PBS, counterstained by applying IFMDD mounting medium (EMS, #17989-97/-98) containing ImmunoMount™ DAPI (4',6-diamido-2-phenylindole) and DABCO™ (1,4-diazobicyclo-(2,2,2)-octane), coverslipped, and examined with a Leica TCS SPEII DMI4000 scanning laser confocal fluorescence microscope, using a 635-nm laser with a laser intensity of 20.9% and arbitrary gain set at 830 to optimize the signal-to-noise ratio. Images were captured using a 40X oil immersion objective (NA 1.15), and stored as TIFF files on a Microsoft Windows®-based computer, then exported to Adobe PhotoShop®.

Statistical analysis

Numerical values for outcomes measures are expressed as mean ± standard error of the mean (SEM). Measures of retinal (ERG) and visual (OMR) function were analyzed using linear mixed models with a single between-subject factor (blast, control) and the two within-subjects factors of time-point (2, 4, 6, and 8 months) and eye (right, left) as fixed effects. These analyses were run with a similar structure to traditional repeated measures analysis of variance (ANOVA; compound symmetry error structure) but made use of all available data to avoid bias. SD-OCT data had an additional factor of quadrant, which was incorporated as an additional random effect (source of dependence). Post hoc comparisons of specific time and group differences, as well as a linear trend test were performed using linear combinations of the appropriate coefficients in the model. Weights and Y-maze results were analyzed using a two-way repeated measures ANOVA followed by a Holm-Sidak test for individual comparisons.

Results

Blast-exposed rats had greater ERG amplitudes and delayed ERG implicit times

ERG waveforms from both eyes of blast-exposed rats had larger amplitudes than those of control rats at all time-points examined. Figure 2 shows representative responses for dark-adapted ERGs (Fig. 2A), dark-adapted OPs (Fig. 2B), and light-adapted flicker (Fig. 2C) from rats 8 months post-blast exposure in comparison with controls. Blast-exposed rats showed greater a-wave amplitudes in both the ipsilateral and contralateral eyes compared with controls (mixed model analysis main effect of group, $F[1,247] = 27.87$, $p < 0.001$; Fig. 3A), and greater b-wave amplitudes (mixed model analysis main effect of group, $F[1,249] = 39.19$, $p < 0.001$; Fig. 3C). Implicit times for a-waves of both eyes of blast-exposed animals were delayed across time (mixed model analysis main effect of group, $F[1,247] = 9.71$, $p < 0.001$; Fig. 3B). At 6 and 8 months post-blast, b-wave implicit times of both eyes of blast-exposed animals showed delays (mixed model analysis two-way [time x group] interaction $F[3,279] = 7.45$, $p < 0.001$; Fig. 3D). OPs recorded in response to the brightest dark-adapted stimuli (2.1 log cd sec/m^2) showed a similar pattern of increased amplitudes and delayed implicit times. OP2 was greater in both eyes of blast-exposed animals (mixed model analysis main effect of group $F[1,247] = 48.29$, $p < 0.001$; Fig. 3E) and had delayed implicit times relative to controls (mixed model analysis main effect of group $F[1,247] = 61.43$, $p < 0.001$; Fig. 3F). All OPs showed the same changes in amplitudes and implicit times as OP2, except OP1 of blast-exposed animals—which only had greater amplitudes but not delayed implicit times relative to controls (data not shown). Light adapted flicker b-wave amplitudes were 25% greater for both eyes of blast-exposed animals relative to

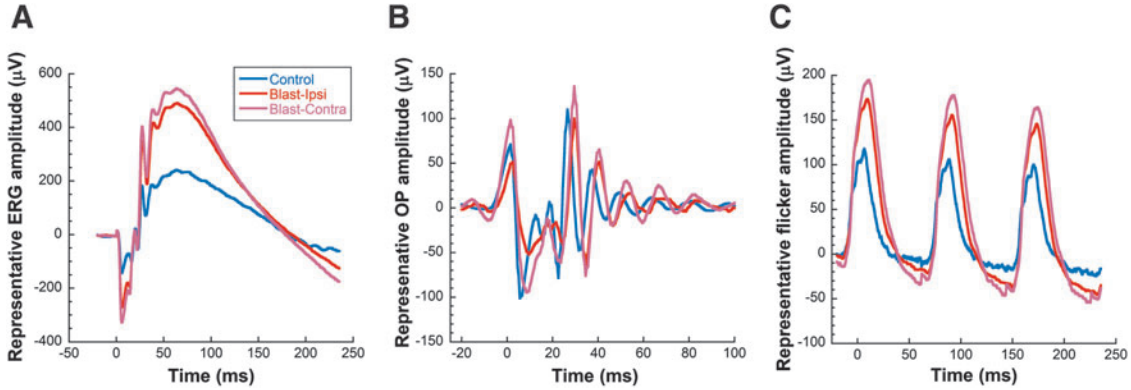

FIG. 2. Representative ERG waveforms from control rats (blue traces) versus ipsilateral (ipsi) and contralateral (contra) eyes from blast-exposed rats (red traces) at 8 months post-blast. Blast-exposed rats exhibit increased amplitudes and delayed implicit times in both ipsilateral and contralateral eyes, compared with age-matched controls. **(A)** Dark-adapted ERGs; **(B)** dark-adapted oscillatory potentials; **(C)** light-adapted flicker responses. ERG, electroretinography.

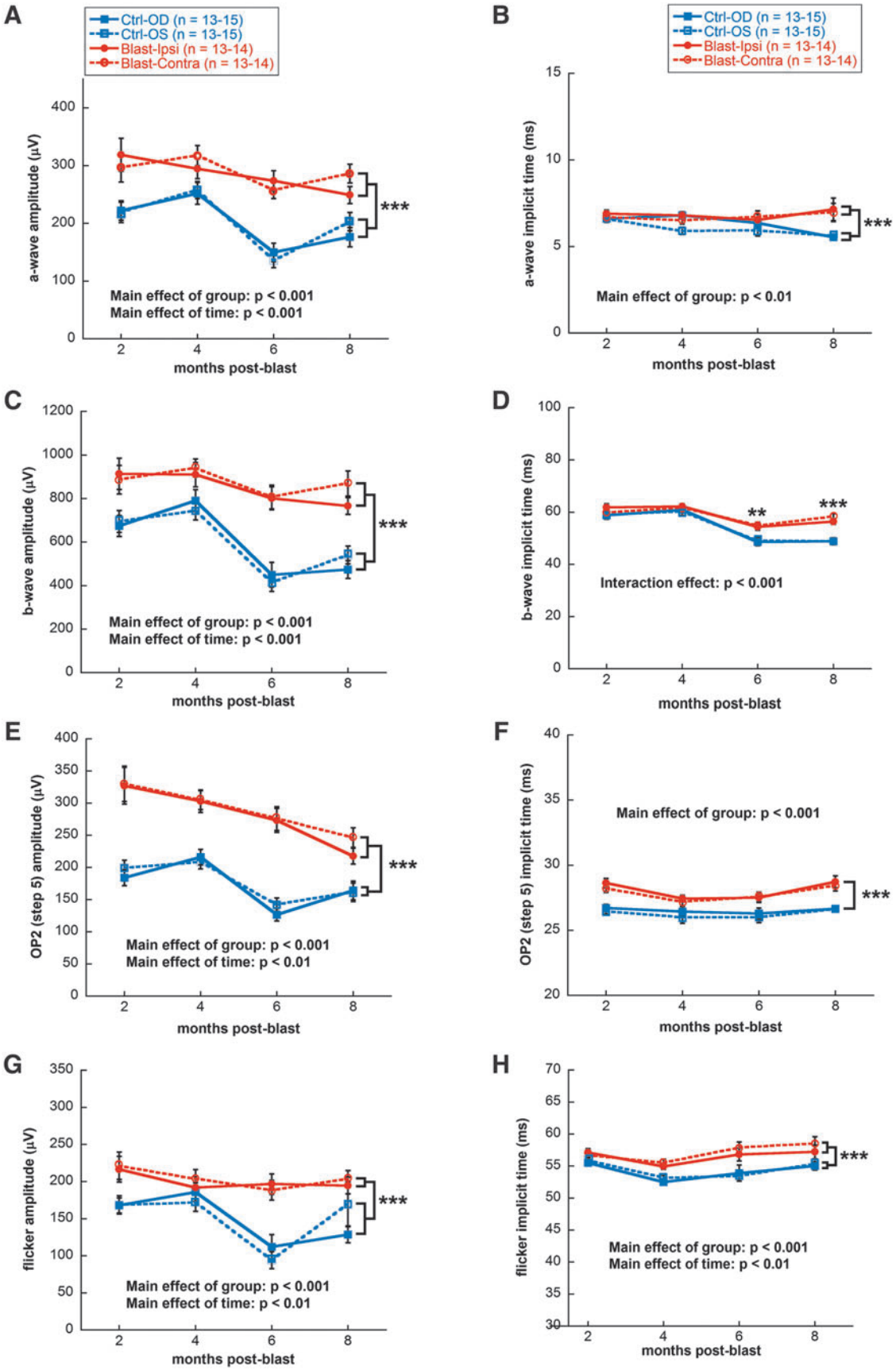

FIG. 3. Quantification of ERG a-wave, b-wave, oscillatory potentials, and flicker response amplitudes and implicit times. Significant increases in dark-adapted a-wave **(A)**, dark-adapted b-wave **(C)**, dark-adapted oscillatory potential **(E)**, and light-adapted flicker **(G)** amplitudes were observed in both ipsilateral (OD) and contralateral (OS) eyes of blast-exposed rats compared with non-blast-exposed controls. Significant delays in dark-adapted a-wave **(B)**, dark-adapted b-wave **(D)**, dark-adapted oscillatory potential **(F)**, and light-adapted flicker implicit times **(H)** were observed in both eyes from blast-exposed rats compared with controls; $***p < 0.001$, $**p < 0.01$. Results expressed as mean ± SEM values. ERG, electroretinography; SEM, standard error of the mean.

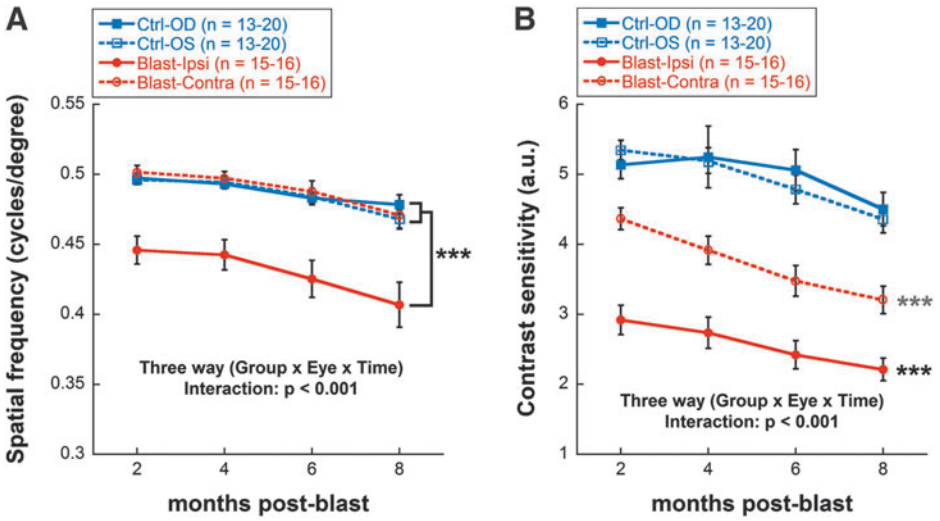

FIG. 4. Reduced spatial frequency and contrast sensitivity in blast-exposed versus control rats. **(A)** Spatial frequency thresholds as a function of post-blast time (2–8 months). **(B)** Contrast sensitivity thresholds as a function of post-blast time (2–8months). Black asterisks indicate comparisons of ipsilateral blast-exposed eyes (OD) with both the contralateral (OS) blast-exposed eyes and both eyes of control rats; blue asterisks indicate comparisons of the contralateral (OS) blast-exposed eyes with both the ipsilateral (OD) blast-exposed eyes and with both eyes of control rats. ***$p < 0.001$. Results expressed as mean ± SEM values. SEM, standard error of the mean.

controls (mixed model analysis main effect of group, $F[1,243] = 19.72$, $p < 0.001$; Fig. 3G). Flicker implicit times also were delayed for both eyes of blast-exposed rats (mixed model analysis main effect of group, $F[1,243] = 16.92$, $p < 0.001$; Fig. 3H).

Blast-exposed rats showed reduced spatial frequency and contrast sensitivity

Both SF and CS thresholds were significantly reduced in blast-exposed animals, compared with non-blast-exposed controls, beginning at 2 months post-blast. SF was only reduced in the ipsilateral blast-exposed eye (20% lower than both the contralateral and control eyes, on average, across time; mixed model analysis three-way interaction effect, $F[4,257] = 21.04$, $p < 0.001$; Fig. 4A). CS outcomes appeared to show greater sensitivity to the blast exposure, with both the ipsilateral and contralateral eyes having reduced CS relative to non-blast-exposed controls (mixed model analysis three-way interaction effect, $F[4,257] = 21.10$, $p < 0.001$; Fig. 4B). By 8 months post-blast, CS for ipsilateral eyes was 50% of control values and CS for contralateral eyes was 72% of control values. In addition to the decrease seen in visual function due to blast exposure, there was an aging effect: both SF (mixed model analysis main effect of time, $F[3,257] = 2.94$, $p = 0.034$) and CS (mixed model analysis main effect of time, $F[3,257] = 5.64$, $p = 0.001$) scores declined over time for all groups.

Blast-exposed rat eyes exhibited increased retinal thickness

Figure 5 shows representative SD-OCT retinal images from control and blast-exposed rats at 4 months post-blast, whereas Figure 6 displays the quantification of thickness measurements for each retinal layer and the whole retina longitudinally. TRT of blast-exposed animals was greater, relative to controls, across all time-points (mixed model analysis main effect of group, $F[1,691] = 68.558$, $p < 0.001$; Fig. 6A). This increase was a composite of changes in

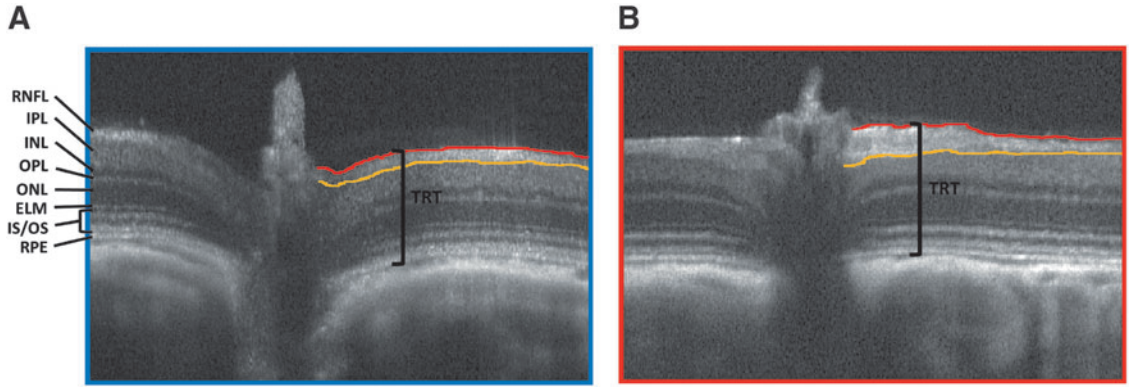

FIG. 5. Representative SD-OCT images taken 4 months post-blast from **(A)** control and **(B)** blast-exposed rats. Lines delineating retinal nerve fiber layer (RNFL) to easily visualize increased layer thickness of blast-exposed eye versus control. Total retinal thickness (TRT) was measured from the top of the RNFL to the bottom of the RPE. ELM, external limiting membrane; INL, inner nuclear layer; IPL, inner plexiform layer; IS/OS, inner segment/outer segment layer; ONL, outer nuclear layer; OPL, outer plexiform layer; RPE, retinal pigment epithelium; SD-OCT, spectral domain–optical coherence tomography.

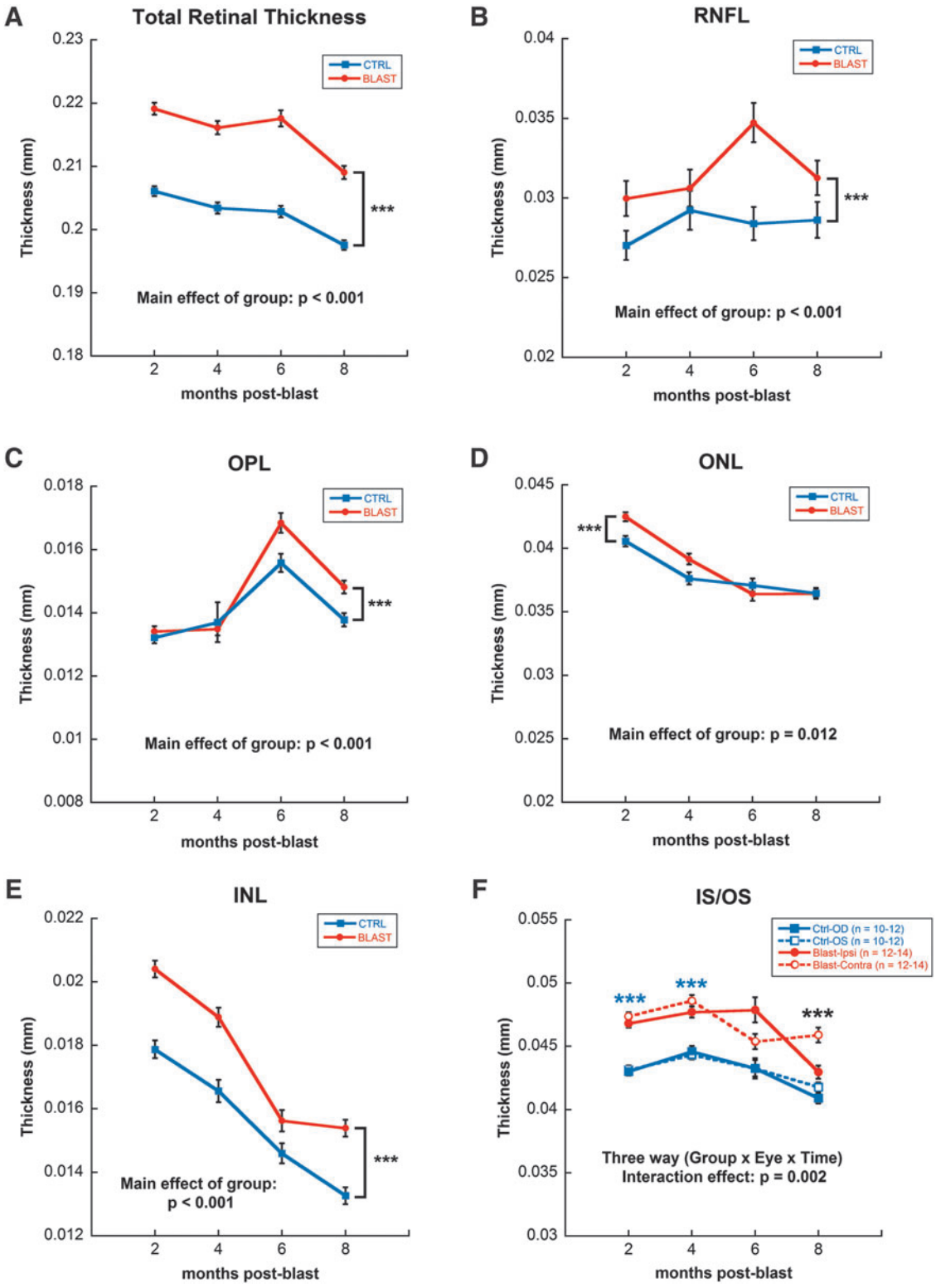

FIG. 6. Quantification of SD-OCT measurements by quadrant and across time. Significant increase in total retinal thickness **(A)** of blast versus control animals (eyes averaged per group) due to increases in individual layers of the retina, including: RNFL **(B)**, OPL **(C)**, ONL **(D)**, INL **(E)** and IS/OS **(F)**. IS/OS showed significant changes in the contralateral eye of blast-exposed animals as well. Blue asterisks indicate comparisons of ipsilateral blast-exposed eyes (OD) and contralateral (OS) blast-exposed eyes with both eyes of control rats; black asterisks indicate comparisons of contralateral (OS) blast-exposed eyes with both the ipsilateral blast-exposed eyes (OD) and with both eyes of control rats. ***$p < 0.001$. Results expressed as mean ± SEM values. INL, inner nuclear layer; IS/OS, inner segment/outer segment layer; ONL, outer nuclear layer; OPL, outer plexiform layer; SD-OCT, spectral domain–optical coherence tomography; SEM, standard error of the mean.

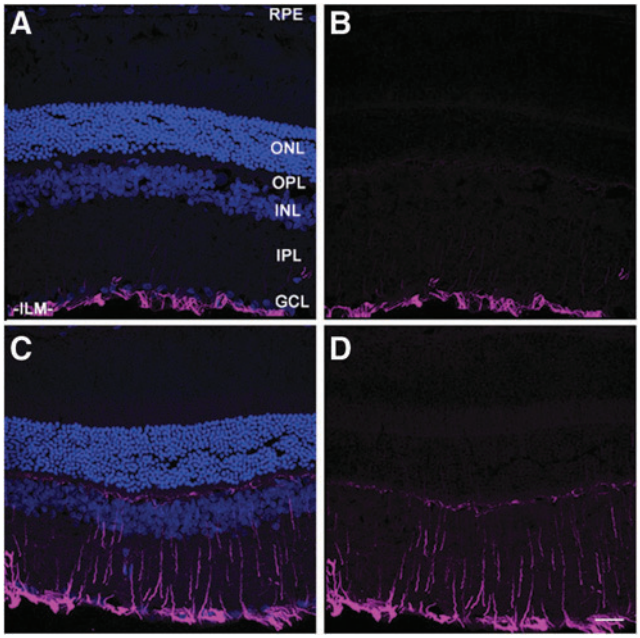

FIG. 7. Marked upregulation and persistence of anti-GFAP immunoreactivity in ipsilateral blast-exposed retina **(C,D)**, relative to non-blast-exposed control **(A,B)**. Frozen tissue sections were immunostained with anti-GFAP, followed by treatment with AlexFluor® 647-conjugated secondary antibody (magenta), and counterstained with DAPI (blue) to label nuclei. Laser confocal fluorescence microscopy images were taken, with (A,C) and without (B,D) the DAPI channel. A representative area of pericentral retina for each condition is shown. Scale bar (panel D), 25 μm. ILM, inner limiting membrane; INL, inner nuclear layer; IPL, inner plexiform layer; GCL, ganglion cell layer; GFAP, glial fibrillary acidic protein; ONL, outer nuclear layer; OPL, outer plexiform layer; RPE, retinal pigment epithelium.

several retinal layers: RNFL (mixed model analysis main effect of group, $F[1,691] = 19.175$, $p < 0.001$), OPL (mixed model analysis main effect of group, $F[1,691] = 27.08$, $p < 0.001$], ONL (mixed model analysis main effect of group, $F[1,691] = 6.44$, $p = 0.012$), and INL (mixed model analysis main effect of group, $F[1,691] = 12.52$, $p < 0.001$; Fig. 6B–E).Within the IS/OS, there was also a difference between both the ipsilateral and contralateral eyes of blast-exposed rats, relative to controls, across time (mixed model analysis three-way interaction, $F[4,691] = 2.43$, $p = 0.002$; Fig. 6F).

Blast-exposed rat eyes exhibited marked upregulation of GFAP

Neuronal injury is often accompanied by gliotic changes, which are typically detected by elevated expression of GFAP.[23,24] We evaluated GFAP expression in the retinas of blast-exposed versus unexposed control eyes, 8 months post-blast, by immunofluorescence histochemistry, probing tissues sections with anti-GFAP antibodies and fluor-conjugated secondary antibodies. Representative micrographs taken from the ipsilateral eye of a blast-exposed animal and an non-blast-exposed control rat are shown in Figure 7. Control retinas exhibited anti-GFAP immunoreactivity almost exclusively in the inner limiting membrane (ILM) and ganglion cell layer (GCL; Fig. 7A,B), corresponding to astrocytes and Müller glia ''endfeet.'' In striking contrast, retinas from blast-exposed eyes (Fig. 7C,D) showed intense anti-GFAP immunolabeling both in the ILM and GCL as well as in a radial pattern that extended deep into the retinal layers, to the OPL and even into the photoreceptor layer. Notably, this demonstrates a strong, blast-induced gliotic response that persisted for up to 8 months after a single blast exposure. Despite this, under the conditions employed, we observed no qualitative thinning of retinal layers, including the inner and outer nuclear layers (INL and ONL, respectively), consistent with the results obtained *in vivo* using SD-OCT imaging (see above). Contralaterals eyes also exhibited elevated GFAP immunoreactivity (not shown), but the label

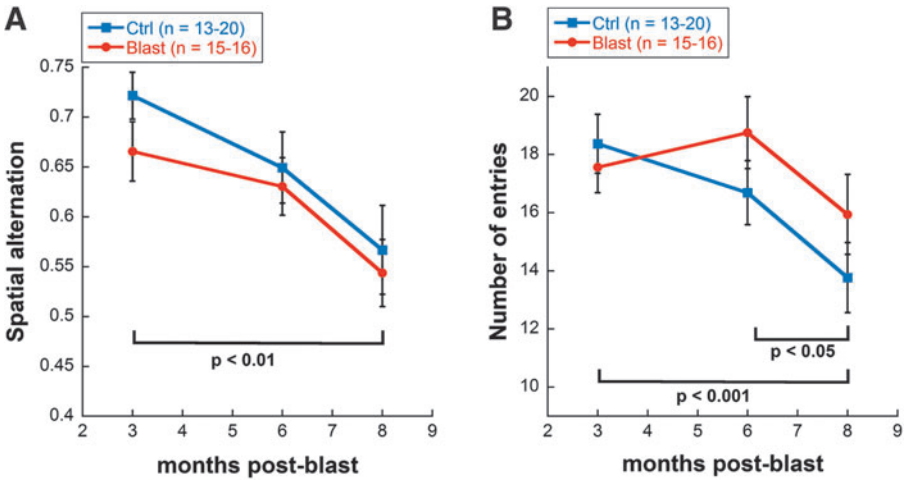

FIG. 8. Y-maze analysis of **(A)** cognitive function and **(B)** exploratory motor behavior of blast-exposed (red trace) versus control rats (blue trace) as a function of post-blast time. Both groups exhibited comparable performance measures, and both groups also exhibited performance decline (deficits) over time. Assessments were made at 3, 6, and 8 months post-blast. Cognitive function was measured by spatial alternation on Y-maze; exploratory motor behavior was measured by number of entries on Y-maze. Results expressed as mean ± SEM values. SEM, standard error of the mean.

tended to be more ''patchy'' in distribution and variable in intensity, compared with the pattern in ipsilateral eyes.

Blast-exposed rats had normal cognitive and exploratory motor behavior

Although there was a trend for decreased spatial alternation in the blast-exposed group at 3 months post-blast, the difference was not statistically significant. By 6 months and up until 8 months, blast-exposed and control animals showed similar spatial alternation scores (spatial cognition), as well as a similar number of entries (exploratory motor behavior). However, spatial alternation decreased with age for both blast-exposed and control animals (two-way repeated measures ANOVA main effect of time, $F[2,94] = 7.41$, $p = 0.001$; Fig. 8A). Total number of entries also decreased with age for both blast-exposed and control rats (two-way repeated measures ANOVA main effect of time, $F[2,95] = 8.23$, $p < 0.001$; Fig. 8B).

Discussion

Long-term visual testing revealed a unique blast-induced phenotype in the retina

Using a relatively novel animal model of ABO exposure, we observed visual deficits persisting up to 8 months post-blast exposure, coupled with a unique retinal phenotype. The combination of thicker retinal layers, increased ERG amplitudes, and delays in implicit times is very atypical of retinal diseases, whether hereditary or environmentally induced. Retinal degenerations typically involve *decreased* ERG amplitudes accompanied by progressive and irreversible retinal thinning, the latter most often involving the degeneration, death, and dropout of photoreceptors.[25] Indeed, it is rare to find visual disorders that present with an *increase* in ERG amplitudes, although such increases have been reported in Ant1-deficient mice,[26] in a rabbit model of retinal degeneration,[27] and in patients with early diabetic retinopathy,[28] in which reduced inhibition from amacrine cells is proposed to increase rod bipolar cell signaling.[29] However, a trend toward larger ERG b-wave V_{max} values has been observed in some patients with blast-induced injuries (S. Viswanathan, SUNY College of Optometry; personal communication, July 2017), supporting the idea that this rat model of ABO injury has clinical relevance for characterizing the mechanisms of ABO-induced retinal injury and developing therapeutic interventions.

Previous research with animal models of primary blast injury has provided valuable information about the development of post-blast retinal pathology, including increases in activated caspase-3[30,31] and caspase-1[13] in the retina and optic nerve, changes in retinal thickness,[15,32,33] and changes in retinal and visual function.[12–16,32–34] However, much of this research was performed over a relatively short post-blast time-course, typically one month or less,[12–16] and the results have been somewhat inconsistent, with ERG amplitudes reported to decrease,[16] increase,[13] or not change at all.[14,33] What appears to be inconsistencies may actually be a differential retinal response during acute and chronic phases after blast injury, with our data representing the chronic phase.

Loss of inhibition may cause supranormal ERG amplitudes

The increased ERG amplitudes we observed in the retina mirror other supranormal increases in excitation observed in the brain after blast injury.[35–37] In the brain, changes in glutamate (the major excitatory neurotransmitter) and gamma aminobutyric acid (GABA; the main inhibitory neurotransmitter) occur in waves after brain injury. Acute changes include differences in GABA-A expression, decreased glutamate transporter expression, and excess glutamate release and excitotoxicity, whereas chronic changes include GABA receptor dysfunction, GABA interneuron cell death, and a growing imbalance between excitation and inhibition.[37] These chronic changes can occur *months* after injury. For example, 20.5% of patients with moderate-to-severe traumatic brain injury (TBI) develop late-onset post-traumatic seizures between 7 days and 5 years post-TBI,[38] which is thought to be due to a shift in the balance of excitation and inihibition.[37] In the amygdala and hippocampus, mild TBI causes reduced inhibition due to loss of GABAergic interneurons, leading to anxiety-like behavior[35]and long-term potentiation deficits,[36] respecitively.

In the retina, GABA and its receptor agonists act to reduce various components of the ERG amplitude, whereas applying GABA receptor antagonists or genetically knocking out GABA receptors results in supranormal ERG amplitude[39–42] (although GABA-C receptor inhibition or knockout is sometimes an exception).[39] Thus, a lack of GABAergic inhibition is capable of driving supranormal amplitudes in various components of the ERG. In addition, spontaneous firing of retinal ganglion cells increases after blast injury,[32] which lends further support to the idea of an imbalance between excitatory and inhibitory pathways that contribute to the overall response of the retina to photic stimulation following ABO exposure.

Because GABAergic amacrine cells have medium-to-large dendritic fields that branch delicately throughout all five inner plexiform layer strata,[43,44] these cells may become more fragile when a blast overpressure wave sweeps through the retina (and possibly also in different retinal disease models). In support of this idea, most of the blast-induced caspase-1 labeling reported by Bricker-Anthony and associates[13] was observed in the cholinergic amacrine cells of the retina. In the brain, axonal pathologies seen after blast exposure are thought to be critical to the progression of visual, cognitive, and motor deficits.[45,46] Future experiments will be aimed at investigating whether GABAergic interneurons in the retina are more sensitive to axonal degeneration after blast, and whether the death of these cells causes a decrease in inhibition that underlies the observed increase in ERG amplitudes.

Blast exposure produces more pronounced deficits in contrast sensitivity than in spatial frequency

Despite having increased ERG amplitudes, blast-exposed rats exhibited deficits in visual function, as measured by OMR. In our model, we presented an ABO insult to the right side of the head; hence, the right eye (OD) was ipsilateral to the shock-wave front, whereas the left eye (OS) was contralateral. Interestingly, although changes in ERG and TRT measurements were observed in both the ipsilateral as well as contralateral eyes of blast-exposed rats (relative to non-blast-exposed controls), OMR analysis revealed the greatest discrepancy between ipsilateral and contralateral eyes. For SF, only ipsilateral eyes showed a deficit. For CS, deficits were more pronounced in ipsilateral than in contralateral eyes. Several factors could be underlying these differences. First, CS measurements may be more sensitive than SF measurements. Second, differences in distribution of cell death and/or morphological changes may explain the differences in blast and contralateral eyes. Contralateral eyes may be less affected because the incident blast wave impacts the contralateral eye with reduced intensity after traveling through and around the ipsilateral eye and skull. Alternatively, the contralateral eye may be damaged by blunt trauma from impact against the wall of the housing

chamber.[14] Third, in addition to interneurons, the optic nerve and retinal ganglion cells are also particularly sensitive to blast injury and mechanical shear stress,[32,33,47] and retinal ganglion cells play an important role in CS.[48,49] Our SD-OCT data showing increased RNFL thickness in blast-exposed rats, relative to controls, supports the idea of retinal ganglion cell involvement. Of note, CS deficits have been shown to be more pronounced than visual acuity deficits after blast injury in humans as well.[9] Future studies are needed to determine precisely what mechanisms are driving changes to the contralalateral eye after blast injury.

Persistence of gliotic response several months after blast exposure

A remarkable and unexpected finding from this study was the long-lived persistence of GFAP upregulation in blast-exposed retinas, even 8 months after a single exposure to ABO. GFAP upregulation is typically a signature that accompanies any insult to the retina, including neuronal degeneration and cell death in retinal degenerative diseases,[23,24] hyperglycemia insult in diabetic retinopathy,[50,51] and ischemic insult in ocular stroke.[52] The persistence of a gliotic response suggests that the local microenvironment of the retina was perturbed by blast exposure, belying the apparent ''normalcy'' of retinal layer thickness. The mechanisms that underlie this persistence in GFAP upregulation are unclear at this time, and remain to be elucidated. The fact that contralateral eyes also exhibited elevated levels of GFAP demonstrates that those eyes were subjected to trauma, and they cannot serve as ''internal controls'' for the effects of ABO exposure (hence, the need to use non-blast-exposed animals as suitable controls). Although several other studies of blast-exposed animals have documented upregulation of GFAP and gliosis in the retina,[12–14] this is the first study to document such long-lived persistence of these changes, particularly under conditions where no overt signs of retinal degenerative changes are apparent.

What causes increased retinal thickness in blast-exposed eyes?

Although there was a decrease in CS in blast-exposed animals compared with controls, we did not find a concurrent thinning of the RNFL; rather, *increased* RNFL thickness was observed by SD-OCT analysis. Further, increased thickness measurements were observed in other layers of the retina (both inner and outer layers), which collectively contributed to an increase in the overall thickness of the retina in blast-exposed eyes relative to controls.

Several studies have reported thinning of the retina in response to blast injury[53,54]; yet, other studies have also reported thickening.[55,56] The severity of the blast overpressure conditions employed may contribute to these differences. We employed a sound pressure level of approximately 190 dB SPL, which converts to a pressure value of about 63 kPa with a backpressure load in the shock tube of 80 psi, to closely mimic mild blast-induced TBI conditions. We chose these conditions to avoid globe rupture, retinal detachment, retinal hemorrhage, traumatic cataract formation, optic nerve shearing, or any other overt blast-induced tissue damage. Most other studies have used >100 kPa,[13,16,31,57] and some >300 kPa,[58,59] which approximate moderate- or severe-grade blast-induced TBI conditions, respectively. Also, differences in the distance between the outlet of the shock tube and the head of the animal (point of impact of the shockwave) have varied from one study to another. Varying severities of injury, especially from low-level blast, have been shown to result in different pathologies.[60,61] With greater insults, more immediate cell death occurs.[16,32,62,63] In addition, at higher levels of blast overpressure, it is more difficult to control for head movement and rotation, which also seems to be a key differentiating factor in injury severity.[64] Mild blast-induced TBI that is below the threshold for immediate cell death, may trigger a neuroinflammatory response to repair damaged tissue, which may explain the persistent increased retinal thickness observed here. Preliminary findings (S.J. Fliesler, unpublished) suggest that resident retinal microglia (Iba-1-positive cells) become activated and migrate from the inner-most to the middle and outer retinal layers following blast exposure, where they may release inflammatory mediators (see also comments below).

Edema may also play a role in the observed blast-induced increase in retinal thickness. Blood–retinal barrier (BRB) permeability can be affected by blast-induced damage to retinal blood vessels[65] and the RPE-choroid complex,[13,14] causing fluid leakage and swelling.[66] Disruption of the RPE-choroid complex may explain the increased thickness we observed in the IS/OS layer of the retina. (Note: We found no qualitative differences in retinal histology at one week post-blast compared with non-blast-exposed controls [unpublished results]. However, given that tissue processing for conventional paraffin or plastic embedment histology involves serial dehydration of tissue specimens, we did not consider it fruitful to pursue assessment of retinal layer thickness differences by this means. Rather, the *in vivo* measurements afforded by SD-OCT provide a more quantitatively accurate and physiologically relevant assessment of tissue dimensions.)

The other specific layer where we saw a significant thickness increase was the INL, which contains the Müller cell bodies. Other studies have noted greater changes in the INL[31] and the Müller cells[31,65,67] with blast, in addition to other glial cells in the retina and brain.[68,69] These findings are consistent with the concept that a persistent inflammatory response is driving the blast-induced increased thickness in the INL and throughout the retina, as observed in this study.

Using the eye as a window to the brain in blast injury

Because retinal neurons are accessible for imaging and functional testing in a way that other neural tissue is not, the retina can be used to provide information about risk, onset, and progression of pathogenesis in a variety of diseases, including stroke, diabetes, Alzheimer's, Parkinson's, multiple sclerosis, schizophrenia, autism, and seasonal affective disorder.[52,70–76] Historically, getting a diagnosis of blast injury has been difficult, especially because PTSD and blast injury can have many overlapping symptoms.[3] Blast injury, like chronic traumatic encephalopathy,[77] has characteristic pathological hallmarks that can be confirmed in postmortem tissue.[78] However, behavioral symptoms of anxiety, sleep disorders, cognitive deficits, seizures, dizziness, and vision changes are more difficult to accurately diagnose and attribute to a specific mechanism.[3] These issues are compounded by the fact that many people who are exposed to ''mild'' blast conditions or concussive trauma often do not receive a full clinical evaluation[6] (often because they self-report that they have no obvious vision problems) and that the effects of blast injury can appear either acutely or chronically, or both.[5,6,37,38,46,79] Our research suggests that a more comprehensive retinal examination, including ERG, SD-OCT, and visual function testing, can be of value in confirming a diagnosis of blast injury, even months after the initiating event of blast exposure has occurred, and in providing a better understanding of the course of blast-induced dysfunction and its underlying mechanisms.

Conclusion

Long-term changes characterized in a novel ABO model revealed increased ERG amplitudes, delays in ERG implicit times, deficits in CS and SF, and increased TRTs. Deficits persisted to 8 months (the longest time-point examined) and were consistent with the types of visual system problems observed in patients who have been exposed to ABO, which supports the validity of this model in studying mechanisms of blast injury and potential treatments.

Acknowledgments

We thank Mary Kelly, PhD, at Emory University for assistance with the statistical analysis. Portions of this work were presented in preliminary form at the 2017 Annual Meeting of the Association for Research in Vision and Ophthalmology (ARVO; May 2017; Baltimore, MD), and at the 6th Military Vision Symposium on Ocular and Vision Injury (March 30–31, 2017; Boston, MA). The opinions expressed herein do not necessarily reflect those of the Department of Veterans Affairs, the National Institutes of Health, or the U.S. Government.

This work was supported, in part, by grants from the National Institutes of Health (NIH) (P30 EY006360 to Emory University [MTP], and NCATS Clinical and Translational Science Award 1UL1 TR001358 to the University at Buffalo [SJF]), and from the Department of Veterans Affairs (BLR&D Service Merit Award 1I01 BX002439 [SJF&MTP]; BLR&D Service Research Career Scientist Award [SJF]; and RR&D Service Research Career Scientist Award [C9257; MTP]).

Author Disclosure Statement

No competing financial interests exist.

References

1. Okie, S. (2005). Traumatic brain injury in the war zone. N. Engl. J. Med. 352, 2043–2047.
2. Defence and Veterans Brain Injury Center. DoD worldwide numbers for TBI. Available at: http://www.dvbic.org/dod-worldwide-numbers-tbi. Accessed July 14, 2017.
3. Goodrich, G.L., Martinsen, G.L., Flyg, H.M., Kirby, J., Garvert, D.W., and Tyler, C.W. (2014). Visual function, traumatic brain injury, and posttraumatic stress disorder. J. Rehabil. Res. Dev. 51, 547–558.
4. Cockerham, G.C., Goodrich, G.L., Weichel, E.D., Orcutt, J.C., Rizzo, J.F., Bower, K.S., and Schuchard, R.A. (2009). Eye and visual function in traumatic brain injury. J. Rehabil. Res. Dev. 46, 811–818.
5. Cockerham, G.C., Rice, T.A., Hewes, E.H., Cockerham, K.P., Lemke, S., Wang, G., Lin, R.C., Glynn-Milley, C. and Zumhagen, L. (2011). Closed-eye ocular injuries in the Iraq and Afghanistan wars. N. Engl. J. Med. 364, 2172–2173.
6. Lemke, S., Cockerham, G.C., Glynn-Milley, C., Lin, R., and Cockerham, K.P. (2016). Automated perimetry and visual dysfunction in blast-related traumatic brain injury. Ophthalmology 123, 415–424.
7. Weichel, E.D., Colyer, M.H., Ludlow, S.E., Bower, K.S., and Eiseman, A.S. (2008). Combat ocular trauma visual outcomes during Operations Iraqi and Enduring Freedom. Ophthalmology 115, 2235–2245.
8. Goodrich, G.L., Kirby, J., Cockerham, G., Ingalla, S.P., and Lew, H.L. (2007). Visual function in patients of a polytrauma rehabilitation center: a descriptive study. J. Rehabil. Res. Dev. 44, 929–936.
9. Coe, C.D., Bower, K.S., Brooks, D.B., Stutzman, R.D., and Hammer, J.B. (2010). Effect of blast trauma and corneal foreign bodies on visual performance. Optom. Vis. Sci. 87, 604–611.
10. Magone, M.T., Kwon, E., and Shin, S.Y. (2014). Chronic visual dysfunction after blast-induced mild traumatic brain injury. J. Rehabil. Res. Dev. 51, 71–80.
11. Goodrich, G.L., Flyg, H.M., Kirby, J.E., Chang, C.Y., and Martinsen, G.L. (2013). Mechanisms of TBI and visual consequences in military and veteran populations. Optom. Vis. Sci. 90, 105–112.
12. Bricker-Anthony, C., Hines-Beard, J., D'Surney, L., and Rex, T.S. (2014). Exacerbation of blast-induced ocular trauma by an immune response. J. Neuroinflamm. 11, 192.
13. Bricker-Anthony, C., Hines-Beard, J., and Rex, T.S. (2014). Molecular changes and vision loss in a mouse model of closed-globe blast trauma. Invest. Ophthalmol. Vis. Sci. 55, 4853–4862.
14. Bricker-Anthony, C., and Rex, T.S. (2015). Neurodegeneration and vision loss after mild blunt trauma in the C57Bl/6 and DBA/2J mouse. PloS One 10, e0131921.
15. Reiner, A., Heldt, S.A., Presley, C.S., Guley, N.H., Elberger, A.J., Deng, Y., D'Surney, L., Rogers, J.T., Ferrell, J., Bu, W., Del Mar, N., Honig, M.G., Gurley, S.N., and Moore, B.M., 2nd. (2014). Motor, visual and emotional deficits in mice after closed-head mild traumatic brain injury are alleviated by the novel CB2 inverse agonist SMM-189. Int. J. Mol. Sci. 16, 758–787.
16. DeMar, J., Sharrow, K., Hill, M., Berman, J., Oliver, T., and Long, J. (2016). Effects of primary blast overpressure on retina and optic tract in rats. Front. Neurol. 7, 59.
17. Newman, A.J., Hayes, S.H., Rao, A.S., Allman, B.L., Manohar, S., Ding, D., Stolzberg, D., Lobarinas, E., Mollendorf, J.C., and Salvi, R. (2015). Low-cost blast wave generator for studies of hearing loss and brain injury: blast wave effects in closed spaces. J. Neurosci. Methods 242, 82–92.
18. Aung, M.H., Kim, M.K., Olson, D.E., Thule, P.M., and Pardue, M.T. (2013). Early visual deficits in streptozotocin-induced diabetic Long Evans rats. Invest. Ophthalmol. Vis. Sci. 54, 1370–1377.
19. Prusky, G.T., Alam, N.M., Beekman, S., and Douglas, R.M. (2004). Rapid quantification of adult and developing mouse spatial vision using a virtual optomotor system. Invest. Ophthalmol. Vis. Sci. 45, 4611–4616.
20. Douglas, R.M., Alam, N.M., Silver, B.D., McGill, T.J., Tschetter, W.W., and Prusky, G.T. (2005). Independent visual threshold measurements in the two eyes of freely moving rats and mice using a virtual-reality optokinetic system. Vis. Neurosci. 22, 677–684.
21. Prusky, G.T., Alam, N.M., and Douglas, R.M. (2006). Enhancement of vision by monocular deprivation in adult mice. J. Neurosci. 26, 11554–11561.
22. Maurice, T., Bayle, J., and Privat, A. (1995). Learning impairment following acute administration of the calcium channel antagonist nimodipine in mice. Behav. Pharmacol. 6, 167–175.
23. Yang, Z., and Wang, K.K. (2015). Glial fibrillary acidic protein: from intermediate filament assembly and gliosis to neurobiomarker. Trends Neurosci. 38, 364–374.
24. Lewis, G.P., and Fisher, S.K. (2003). Up-regulation of glial fibrillary acidic protein in response to retinal injury: its potential role in glial remodeling and a comparison to vimentin expression. Int. Rev. Cytol. 230, 263–290.
25. Chang, B., Hawes, N.L., Pardue, M.T., German, A.M., Hurd, R.E., Davisson, M.T., Nusinowitz, S., Rengarajan, K., Boyd, A.P., Sidney, S.S., Phillips, M.J., Stewart, R.E., Chaudhury, R., Nickerson, J.M., Heckenlively, J.R., and Boatright, J.H. (2007). Two mouse retinal degenerations caused by missense mutations in the beta-subunit of rod cGMP phosphodiesterase gene. Vis. Res. 47, 624–633.
26. Phillips, M.J., Webb-Wood, S., Faulkner, A.E., Jabbar, S.B., Biousse, V., Newman, N.J., Do, V.T., Boatright, J.H., Wallace, D.C., and Pardue, M.T. (2010). Retinal function and structure in Ant1-deficient mice. Invest. Ophthalmol. Vis. Sci. 51, 6744–6752.
27. Sakai, T., Kondo, M., Ueno, S., Koyasu, T., Komeima, K., and Terasaki, H. (2009). Supernormal ERG oscillatory potentials in transgenic rabbit with rhodopsin P347L mutation and retinal degeneration. Invest. Ophthalmol. Vis. Sci. 50, 4402–4409.
28. Jenkins, T.C., and Cartwright, J.P. (1990). The electroretinogram in minimal diabetic retinopathy. Bri. J. Ophthalmol. 74, 681–684.
29. Moore-Dotson, J.M., Beckman, J.J., Mazade, R.E., Hoon, M., Bernstein, A.S., Romero-Aleshire, M.J., Brooks, H.L., and Eggers, E.D. (2016). Early retinal neuronal dysfunction in diabetic mice: reduced light-evoked inhibition increases rod pathway signaling. Invest. Ophthalmol. Vis. Sci. 57, 1418–1430.
30. Choi, J.H., Greene, W.A., Johnson, A.J., Chavko, M., Cleland, J.M., McCarron, R.M., and Wang, H.C. (2015). Pathophysiology of blast-induced ocular trauma in rats after repeated exposure to low-level blast overpressure. Clin. Exp. Ophthalmol. 43, 239–246.
31. Wang, H.C., Choi, J.H., Greene, W.A., Plamper, M.L., Cortez, H.E., Chavko, M., Li, Y., Dalle Lucca, J.J., and Johnson, A.J. (2014). Pathophysiology of blast-induced ocular trauma with apoptosis in the retina and optic nerve. Milit. Med. 179, 34–40.

32. Dutca, L.M., Stasheff, S.F., Hedberg-Buenz, A., Rudd, D.S., Batra, N., Blodi, F.R., Yorek, M.S., Yin, T., Shankar, M., Herlein, J.A., Naidoo, J., Morlock, L., Williams, N., Kardon, R.H., Anderson, M.G., Pieper, A.A., and Harper, M.M. (2014). Early detection of subclinical visual damage after blast-mediated TBI enables prevention of chronic visual deficit by treatment with P7C3-S243. Invest. Ophthalmol. Vis. Sci. 55, 8330–8341.
33. Mohan, K., Kecova, H., Hernandez-Merino, E., Kardon, R.H., and Harper, M.M. (2013). Retinal ganglion cell damage in an experimental rodent model of blast-mediated traumatic brain injury. Invest. Ophthalmol. Vis. Sci. 54, 3440–3450.
34. Guley, N.H., Rogers, J.T., Del Mar, N.A., Deng, Y., Islam, R.M., D'Surney, L., Ferrell, J., Deng, B., Hines-Beard, J., Bu, W., Ren, H., Elberger, A.J., Marchetta, J.G., Rex, T.S., Honig, M.G., and Reiner, A. (2016). A novel closed-head model of mild traumatic brain injury using focal primary overpressure blast to the cranium in mice. J. Neurotrauma 33, 403–422.
35. Almeida-Suhett, C.P., Prager, E.M., Pidoplichko, V., Figueiredo, T.H., Marini, A.M., Li, Z., Eiden, L.E., and Braga, M.F. (2014). Reduced GABAergic inhibition in the basolateral amygdala and the development of anxiety-like behaviors after mild traumatic brain injury. PloS One 9, e102627.
36. Almeida-Suhett, C.P., Prager, E.M., Pidoplichko, V., Figueiredo, T.H., Marini, A.M., Li, Z., Eiden, L.E., and Braga, M.F. (2015). GABAergic interneuronal loss and reduced inhibitory synaptic transmission in the hippocampal CA1 region after mild traumatic brain injury. Exp. Neurol. 273, 11–23.
37. Guerriero, R.M., Giza, C.C., and Rotenberg, A. (2015). Glutamate and GABA imbalance following traumatic brain injury. Curr. Neurol. Neurosci. Rep. 15, 27.
38. Ritter, A.C., Wagner, A.K., Fabio, A., Pugh, M.J., Walker, W.C., Szaflarski, J.P., Zafonte, R.D., Brown, A.W., Hammond, F.M., Bushnik, T., Johnson-Greene, D., Shea, T., Krellman, J.W., Rosenthal, J.A., and Dreer, L.E. (2016). Incidence and risk factors of posttraumatic seizures following traumatic brain injury: a traumatic brain injury model systems study. Epilepsia 57, 1968–1977.
39. Moller, A., and Eysteinsson, T. (2003). Modulation of the components of the rat dark-adapted electroretinogram by the three subtypes of GABA receptors. Vis. Neurosci. 20, 535–542.
40. Kupenova, P., Popova, E., and Vitanova, L. (2008). GABAa and GABAc receptor mediated influences on the intensity-response functions of the b- and d-wave in the frog ERG. Vis. Res. 48, 882–892.
41. Behrend, K., Benkner, B., and Mora-Ferrer, C. (2007). Temporal resolution and temporal transfer properties: gabaergic and cholinergic mechanisms. Vis. Neurosci. 24, 787–797.
42. Eggers, E.D., and Lukasiewicz, P.D. (2006). GABAA, GABAC and glycine receptor-mediated inhibition differentially affects light-evoked signalling from mouse retinal rod bipolar cells. J. Physiol. 572, 215–225.
43. Wassle, H., and Boycott, B.B. (1991). Functional architecture of the mammalian retina. Physiol. Rev. 71, 447–480.
44. Pourcho, R.G., and Goebel, D.J. (1983). Neuronal subpopulations in cat retina which accumulate the GABA agonist, (3H)muscimol: a combined Golgi and autoradiographic study. J. Comp. Neurol. 219, 25–35.
45. Yin, T.C., Voorhees, J.R., Genova, R.M., Davis, K.C., Madison, A.M., Britt, J.K., Cintron-Perez, C.J., McDaniel, L., Harper, M.M., and Pieper, A.A. (2016). Acute axonal degeneration drives development of cognitive, motor, and visual deficits after blast-mediated traumatic brain injury in mice. eNeuro 3.
46. del Mar, N., von Buttlar, X., Yu, A.S., Guley, N.H., Reiner, A., and Honig, M.G. (2015). A novel closed-body model of spinal cord injury caused by high-pressure air blasts produces extensive axonal injury and motor impairments. Exp. Neurol. 271, 53–71.
47. Jiang, Y., Liu, L., Pagadala, J., Miller, D.D., and Steinle, J.J. (2013). Compound 49b protects against blast-induced retinal injury. J. Neuroinflamm. 10, 96.
48. Kaplan, E., and Shapley, R.M. (1986). The primate retina contains two types of ganglion cells, with high and low contrast sensitivity. Proc. Natl. Acad. Sci. U S A 83, 2755–2757.
49. Heywod, C.A., Silveira, L.C., and Cowey, A. (1988). Contrast sensitivity in rats with increased or decreased numbers of retinal ganglion cells. Exp. Brain Res. 70, 513–526.
50. Fernandez-Bueno, I., Jones, R., Soriano-Romani, L., Lopez-Garcia, A., Galvin, O., Cheetham, S., and Diebold, Y. (2017). Histologic characterization of retina neuroglia modifications in diabetic zucker diabetic fatty rats. Invest. Ophthalmol. Vis. Sci. 58, 4925–4933.
51. Hernandez-Ramirez, E., Sanchez-Chavez, G., Estrella-Salazar, L.A., and Salceda, R. (2017). Nitrosative stress in the rat retina at the onset of streptozotocin-induced diabetes. Cell. Physiol. Biochem. 42, 2353–2363.
52. Allen, R.S., Olsen, T.W., Sayeed, I., Cale, H.A., Morrison, K.C., Oumarbaeva, Y., Lucaciu, I., Boatright, J.H., Pardue, M.T., and Stein, D.G. (2015). Progesterone treatment in two rat models of ocular ischemia. Invest. Ophthalmol. Vis. Sci. 56, 2880–2891.
53. Hines-Beard, J., Marchetta, J., Gordon, S., Chaum, E., Geisert, E.E., and Rex, T.S. (2012). A mouse model of ocular blast injury that induces closed globe anterior and posterior pole damage. Exp. Eye Res. 99, 63–70.
54. Guley, N.M. (2016). *Mild Traumatic Brain Injury with Associated Visual System Dysfunction: Investigating Histopathology, Functional Correlates, and a Novel Therapeutic Immune Modulator* [dissertation]. University of Tennessee.
55. Zou, Y.-Y., Kan, E.M., Lu, J., Ng, K.C., Tan, M.H., Yao, L., and Ling, E.-A. (2013). Primary blast injury-induced lesions in the retina of adult rats. J. Neuroinflamm. 10, 79–79.
56. Jones, K., Choi, J.H., Sponsel, W.E., Gray, W., Groth, S.L., Glickman, R.D., Lund, B.J., and Reilly, M.A. (2016). Low-Level Primary Blast Causes Acute Ocular Trauma in Rabbits. J. Neurotrauma 33, 1194–1201.
57. Bricker-Anthony, C., D'Surney, L., Lunn, B., Hines-Beard, J., Jo, M., Bernardo-Colon, A., and Rex, T.S. (2017). Erythropoietin either prevents or exacerbates retinal damage from eye trauma depending on treatment timing. Optom. Vis. Sci. 94, 20–32.
58. Svetlov, S.I., Prima, V., Kirk, D.R., Gutierrez, H., Curley, K.C., Hayes, R.L., and Wang, K.K. (2010). Morphologic and biochemical characterization of brain injury in a model of controlled blast overpressure exposure. J. Trauma 69, 795–804.
59. Hart, S., Wang, X., Rex, T., and Geisert, E. (2013). Biomarkers for neuronal injury following blast trauma to the eye. Invest. Ophthalmol. Vis. Sci. 54, 1583–1583.
60. Mishra, V., Skotak, M., Schuetz, H., Heller, A., Haorah, J., and Chandra, N. (2016). Primary blast causes mild, moderate, severe and lethal TBI with increasing blast overpressures: experimental rat injury model. Sci. Rep. 6, 26992.
61. Elder, G.A., Stone, J.R., and Ahlers, S.T. (2014). Effects of low-level blast exposure on the nervous system: is there really a controversy? Front. Neurol. 5, 269.
62. Mammadova, N., Ghaisas, S., Zenitsky, G., Sakaguchi, D.S., Kanthasamy, A.G., Greenlee, J.J., and West Greenlee, M.H. (2017). Lasting retinal injury in a mouse model of blast-induced trauma. Am. J. Pathol. 187, 1459–1472.
63. Petras, J.M., Bauman, R.A., and Elsayed, N.M. (1997). Visual system degeneration induced by blast overpressure. Toxicology 121, 41–49.
64. Risling, M., Plantman, S., Angeria, M., Rostami, E., Bellander, B.M., Kirkegaard, M., Arborelius, U., and Davidsson, J. (2011). Mechanisms of blast induced brain injuries, experimental studies in rats. Neuroimage 54, S89–S97.
65. Zou, Y.Y., Kan, E.M., Lu, J., Ng, K.C., Tan, M.H., Yao, L., and Ling, E.A. (2013). Primary blast injury-induced lesions in the retina of adult rats. J. Neuroinflamm. 10, 79.
66. Cunha-Vaz, J. (2017). The Blood-retinal barrier in the management of retinal disease: EURETINA Award Lecture. Ophthalmologica 237, 1–10.
67. Elder, G.A., Gama Sosa, M.A., De Gasperi, R., Stone, J.R., Dickstein, D.L., Haghighi, F., Hof, P.R., and Ahlers, S.T. (2015). Vascular and inflammatory factors in the pathophysiology of blast-induced brain injury. Front. Neurol. 6, 48.
68. Goodrich, J.A., Kim, J.H., Situ, R., Taylor, W., Westmoreland, T., Du, F., Parks, S., Ling, G., Hwang, J.Y., Rapuano, A., Bandak, F.A., and de Lanerolle, N.C. (2016). Neuronal and glial changes in the brain resulting from explosive blast in an experimental model. Acta Neuropathol. Commun. 4, 124.
69. Kallakuri, S., Desai, A., Feng, K., Tummala, S., Saif, T., Chen, C., Zhang, L., Cavanaugh, J.M., and King, A.I. (2017). Neuronal injury and glial changes are hallmarks of open field blast exposure in swine frontal lobe. PloS One 12, e0169239.
70. Polo, V., Rodrigo, M.J., Garcia-Martin, E., Otin, S., Larrosa, J.M., Fuertes, M.I., Bambo, M.P., Pablo, L.E., and Satue, M. (2017). Visual dysfunction and its correlation with retinal changes in patients with Alzheimer's disease. Eye (London, England) 31, 1034–1041.

71. Emberti Gialloreti, L., Pardini, M., Benassi, F., Marciano, S., Amore, M., Mutolo, M.G., Porfirio, M.C., and Curatolo, P. (2014). Reduction in retinal nerve fiber layer thickness in young adults with autism spectrum disorders. J. Autism Dev. Disord. 44, 873–882.
72. Lavoie, J., Maziade, M., and Hebert, M. (2014). The brain through the retina: the flash electroretinogram as a tool to investigate psychiatric disorders. Prog. Neuropsychopharmacol. Biol. Psychiatry 48, 129–134.
73. Balcer, L.J., and Frohman, E.M. (2010). Evaluating loss of visual function in multiple sclerosis as measured by low-contrast letter acuity. Neurology 74, Suppl. 3, S16–S23.
74. Lee, J.Y., Ahn, J., Kim, T.W., and Jeon, B.S. (2014). Optical coherence tomography in Parkinson's disease: is the retina a biomarker? J. Parkinson's Dis. 4, 197–204.
75. Allen, R.S., Sayeed, I., Oumarbaeva, Y., Morrison, K.C., Choi, P.H., Pardue, M.T., and Stein, D.G. (2016). Progesterone treatment shows greater protection in brain vs. retina in a rat model of middle cerebral artery occlusion: progesterone receptor levels may play an important role. Restor. Neurol. Neurosci. 34, 947–963.
76. Haan, M., Espeland, M.A., Klein, B.E., Casanova, R., Gaussoin, S.A., Jackson, R.D., Millen, A.E., Resnick, S.M., Rossouw, J.E., Shumaker, S.A., Wallace, R., and Yaffe, K. (2012). Cognitive function and retinal and ischemic brain changes: the Women's Health Initiative. Neurology 78, 942–949.
77. Daneshvar, D.H., Goldstein, L.E., Kiernan, P.T., Stein, T.D., and McKee, A.C. (2015). Post-traumatic neurodegeneration and chronic traumatic encephalopathy. Mol. Cell. Neurosci. 66, 81–90.
78. Goldstein, L.E., Fisher, A.M., Tagge, C.A., Zhang, X.L., Velisek, L., Sullivan, J.A., Upreti, C., Kracht, J.M., Ericsson, M., Wojnarowicz, M.W., Goletiani, C.J., Maglakelidze, G.M., Casey, N., Moncaster, J.A., Minaeva, O., Moir, R.D., Nowinski, C.J., Stern, R.A., Cantu, R.C., Geiling, J., Blusztajn, J.K., Wolozin, B.L., Ikezu, T., Stein, T.D., Budson, A.E., Kowall, N.W., Chargin, D., Sharon, A., Saman, S., Hall, G.F., Moss, W.C., Cleveland, R.O., Tanzi, R.E., Stanton, P.K., and McKee, A.C. (2012). Chronic traumatic encephalopathy in blast-exposed military veterans and a blast neurotrauma mouse model. Sci. Trans. Med. 4, 134ra160.
79. Keret, A., Bennett-Back, O., Rosenthal, G., Gilboa, T., Shweiki, M., Shoshan, Y., and Benifla, M. (2017). Posttraumatic epilepsy: long-term follow-up of children with mild traumatic brain injury. J. Neurosurg. Pediatr. 20, 64–70.

Address correspondence to:
Machelle T. Pardue, PhD
Atlanta VA Center for Visual and Neurocognitive Rehabilitation
Research Service (151 Oph)
1670 Clairmont Road
Decatur, GA 30033

E-mail: machelle.pardue@bme.gatech.edu